


## Highly Charged Rydberg Ions from the Coulomb Explosion of Clusters

D. Komar, L. Kazak, M. Almassarani, K-H. Meiwes-Broer, and J. Tiggesbäumker\*  
*Institut für Physik, Universität Rostock, 18059 Rostock, Germany*

 (Received 13 July 2017; published 30 March 2018)

Ion emission from a nanoplasma produced in the interaction of intense optical laser pulses with argon clusters is studied resolving simultaneously charge states and recoil energies. By applying appropriate static electric fields we observe that a significant fraction of the ions  $\text{Ar}^{q+}$  ( $q = 1-7$ ) has electrons with binding energies lower than 150 meV; i.e.,  $n_{\text{Ryd}} \geq 15$  levels are populated. Charge state changes observed on a  $\mu\text{s}$  time scale can be attributed to electron emission due to autoionizing Rydberg states, indicating that high- $\ell$  Rydberg levels are populated as well. The experiments support theoretical predictions that a significant fraction of delocalized electrons, which are bound with hundreds of eV to the nanoplasma after the laser exposure, fill up meV bound ion states in the adiabatic expansion. We expect the process to be relevant for the long-term evolution of expanding laser-induced dense plasmas in general.

DOI: 10.1103/PhysRevLett.120.133207

Since early studies by McPherson *et al.* [1] nanoparticles have served as model targets to study the interaction of finite many-body systems with strong laser fields. Their features are high energy absorption [2], emission of fast electrons [3,4], energetic and highly charged ions [5–7], as well as soft and hard xray photons [8,9]. To explain these phenomena, quasiclassical molecular dynamics simulations are extensively used [10,11]. A variety of effects have been discussed like charging dynamics, expansion, cooling of the nanoplasma, or the directed emission of fast electrons due to resonantly driven collective excitations [12,13]. Recently, spatiotemporal control of electron emission up to keV energies was achieved on attosecond time scales by two-color fields [14].

It is generally accepted that the interaction of clusters with intense optical laser pulses ( $I_L \sim 10^{13}-10^{16}$  W/cm<sup>2</sup>) can be described in a simplified representation by a multistep model [11]. In the rising edge of the pulse, electrons are removed from the cluster by tunnel and barrier suppression ionization. Because of the uncompensated positive charge, a mean field potential builds up. The resulting suppression of direct laser-induced electron emission combined with heating through inverse bremsstrahlung and electron impact excitation transforms the target into a hot and expanding nanoplasma. Within the laser pulse the depth of the confining potential may reach values of keV trapping the delocalized electron cloud, see Fig. 1, left. Molecular dynamic simulations show that during the expansion the overwhelming majority of initially hot electrons in the plasma cloud does not recombine into core levels of multiply charged ions, but appears to be bound with energies less than 50 meV [15]. Hence, an ensemble of highly charged Rydberg ions might be formed, see Fig. 1, right. In a way, the mechanism resembles the formation of Rydberg atoms in an expanding ultracold neutral plasma [16]. In the present studies, the formation

of highly charged Rydberg ions is the focus. The existence of weakly bound electrons in neutrals and weakly charged ions up to  $q = 2$  from cluster Coulomb explosion (CCE) has been demonstrated before by photoelectron studies [17,18]. However, so far it is neither clear whether a Rydberg compound is formed in case of stronger cluster charging, nor how the occupation of Rydberg states influences the experimental observables. Simulations predict that field ionization by spectrometer extraction fields might have a severe impact on the measured charge state distribution [15]. In order to resolve these issues we investigate the occurrence of ions with weakly bound electrons ( $E_B < 150$  meV) produced in the CCE. Unlike other studies [17,18] our diagnostics map the distribution after disintegration of the nanoplasma into well-separated ions.

In the experiments, we use a previously developed charge-state resolving ion energy analyzer (CRIEA) in order to investigate the ion dynamics of the CCE. Its operation principle is described in detail elsewhere [19]. Shortly after

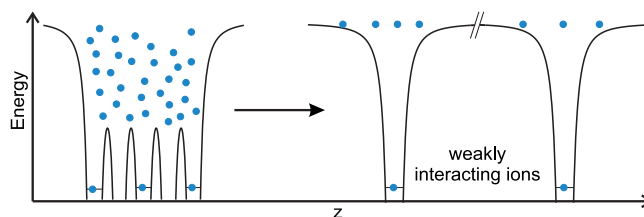


FIG. 1. Temporal evolution of a laser-induced nanoplasma (left: directly after laser exposure, right: after plasma disintegration). In the adiabatic expansion of the plasma ball the delocalized electrons cool down and the ionic potential flattens. A major fraction of the initially hot electrons bound by the keV-deep plasma potential do not recombine into core levels but find themselves finally in low binding energy states (meV) of highly charged ions.

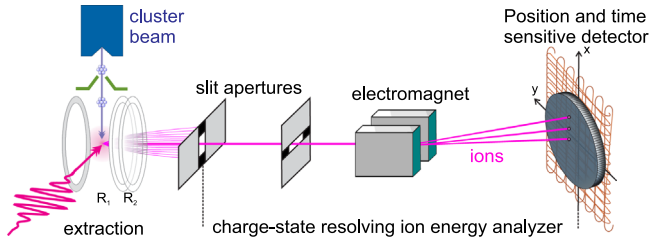


FIG. 2. Schematic view of the experimental setup. Argon clusters exposed to femtosecond laser pulses undergo Coulomb explosion. The ion detection system contains a charge-state resolving ion energy analyzer [19]. To verify the presence of electrons in high lying states of ions, the original setup has been extended by an extraction unit consisting of two electric field regions ( $R_1$ ,  $R_2$ ). In  $R_1$ , ions are accelerated towards the detector. The stronger static field in  $R_2$ , in addition, releases weakly bound electrons.

passing collimating slits, ions from the CCE enter a static magnetic field region where the particles are deflected with respect to their  $q/m$  ratios and kinetic energies. Deflection and arrival times are resolved using a time and position sensitive delay line detector. Plotting the impact position on the detector vs time, time-of-flight–deflection (TOF-deflection) histograms are recorded from which the energy and the charge state of the ions can be deduced. To detect ions with Rydberg electrons we extended the setup by adding two electric field regions ( $R_1$ ,  $R_2$ ), see Fig. 2. Ions are accelerated towards the detector by an extraction field in  $R_1$ , that imprints their initial charge states into the kinetic energy spectra. A higher potential drop in  $R_2$  is applied to release Rydberg electrons. The final charge states and energies are analyzed by the CRIEA. Since the energy gains in  $R_1$  and  $R_2$  depend on the ion charge state in each of these regions, the ions which undergo field ionization within  $R_2$  can be identified in the TOF-deflection histogram. Note, that electrons close to the vacuum level are removed by  $E_1$  (to be discussed below).

Clusters are produced by supersonic expansion of cryogenically cooled Ar gas using a pulsed Even-Lavie valve [20]. The mean cluster size was estimated using the empirical Hagena scaling parameter [21]. To ensure collision-free conditions for the ions when propagating towards the detector, a differential pumping stage is introduced. Entering the interaction region the clusters are exposed to laser pulses at peak intensities of  $I_L = 4 \times 10^{14}$  W/cm<sup>2</sup> within the focus at a central wavelength of 793 nm and a pulse duration of 180 fs, polarized parallel to the spectrometer axis. The extraction unit consists of high transmission meshes separated by 10 and 3 mm, respectively. We recorded TOF-deflection histograms in two different acceleration modes. In Fig. 3, left, only the extraction field ( $E_1 = 100$  V/cm) in  $R_1$  is applied (see inset). In Fig. 3, right, an additional but higher field ( $E_2 = 375$  V/cm) in  $R_2$  releases electrons from highly charged ions (HCIs) nanoseconds after the laser impact.

Each TOF-deflection histogram includes many features, which can be unraveled by a comparison to ion trajectory simulations using SIMION [22]. In Fig. 3, left, strong double-tail structures correspond to ions with different charge states. The calculated TOF and deflections of initially resting ions ( $\text{Ar}^{q+}$ ) are represented by orange circles. The tails which extend to shorter TOF and weaker deflection reflect high ion recoil energies (up to 6 keV) and correspond to  $\text{Ar}^{q+}$  initially emitted either in forward or backward direction with respect to the detector (see inset). When the ionizing field in region  $R_2$  is applied (Fig. 3, right), the double tail structures get shifted in TOF as well as deflection and their shape is significantly modified: the tails shrink and the backward emitted ions get focused in time. Moreover, additional signatures ( $q^F$ ) show up for  $q = 1-6$  as indicated by the red circles. We trace this back to ions having weakly bound electrons. When entering ( $R_2$ ) the tail of the Coulomb potential is bent by the presence of the stronger static electric field and loosely bound electrons are released. Hence, the final velocity of ( $q$ ) and ( $q^F$ ) differ by the charge state dependent energy gain the particles acquire in ( $R_2$ ) resulting in a shift to shorter TOF and stronger deflection so that the ( $q^F$ ) pattern partially overlaps with ( $q + 1$ ). For example, singly charged ions field ionized in  $R_2$  contribute to feature  $1^F$ , see black arrow in Fig. 3, right. The signals of unaffected and field-ionized species agree well with the patterns calculated by the ion trajectory simulations (see up-right inset). Whether more than a single electron is present in these high lying states cannot clearly be established. The corresponding signals would be too close to ( $q^F$ ) to be resolved by the method.

In Fig. 3 additional pronounced features show up at the stronger deflection marked as ( $q^A$ ). For example, in Fig. 3, left, the feature  $1^A$  appears at the time of flight as  $\text{Ar}^{1+}$  (vertical black arrow) but has a different deflection angle with respect to  $q = 1$ . The tilt of the corresponding spectrum of  $1^A$ , indicated by the dashed green line, identifies these species as being in a final charge state  $q = 2$ . Similar features are obtained for all charge states up to  $q = 5$ . The signatures can be attributed to ions emitting an electron in the field-free region in between the extraction region and electromagnet (see Fig. 2), hence, a long time after the interaction. The computed values (blue circles) support these assignments. We also checked whether double ionization contributes but no signals are present at the expected positions.

Whereas the yields of species ionized in the field free region  $q^A$  can clearly be determined, the signals of field-ionized ions  $q^F$  partially overlap with those of the unaffected ions (see upper inset in Fig. 3, right). In order to obtain an estimate on the contribution to the total signal of a given  $q$ , we extract the yields of backward emitted ions. These signals manifest as nearly vertical lines at longer time of flight and do not overlap with the unaffected ions. By taking this as a quantitative measure we determine the specific yields as a function of  $q$ , i.e.,  $Y(q^A)$ ,  $Y(q^F)$ . The result of the analysis is shown in Fig. 4, left. For the total fraction of ions which

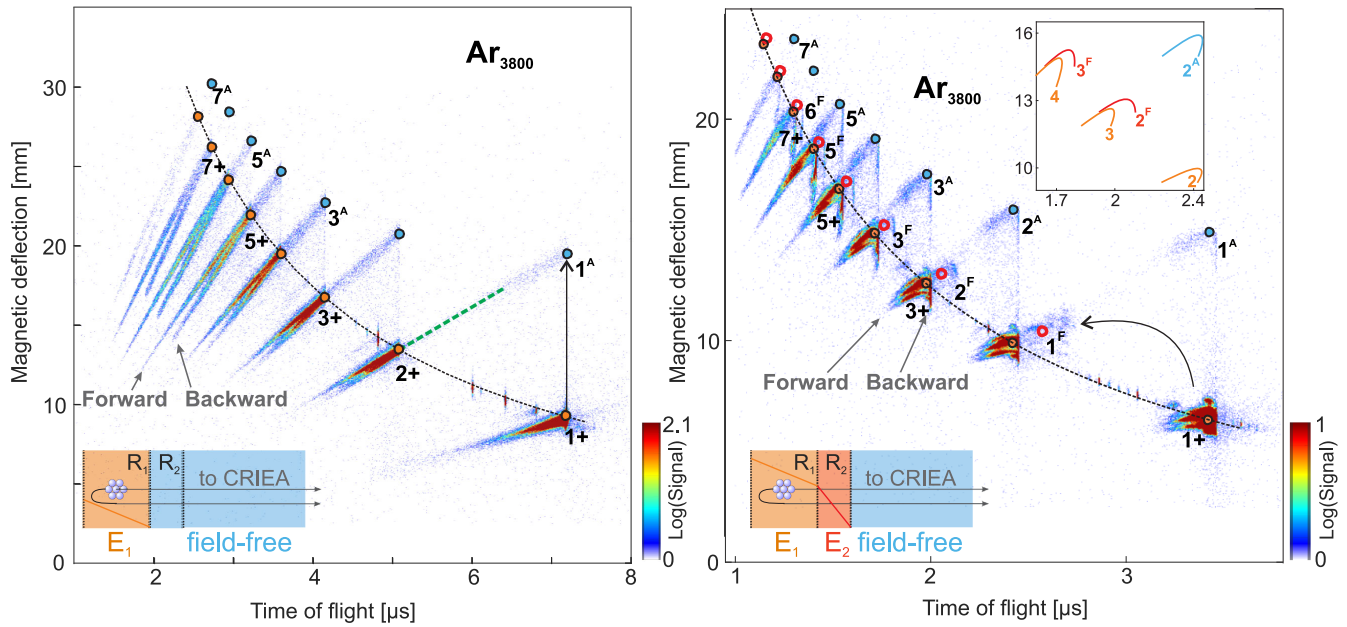


FIG. 3. TOF-deflection histograms of energetic ions from the Coulomb explosion of argon clusters ( $N_{\text{avg}} = 3800$ ) exposed to femtosecond laser pulses ( $I_L = 2 \times 10^{14}$  W/cm $^2$ ). The double tail structures stem from the TOF difference of ions emitted towards and backwards with respect to the detector, see lower insets. Additional static extraction fields allow us to identify products resulting from autoionization ( $q^A = 1^A-5^A$ ) as well as field ionization ( $q^F = 1^F-6^F$ ). Included in the figures are the calculated TOF and magnetic deflections for ions (circles) initially at rest but different  $q/m$  ratios including species which change their charge state on the way to the detector (orange:  $q$ ; blue:  $q^A$ ; red:  $q^F$ ). Note, that as  $q^A$  and  $q^F$  we designate ions being in charge state  $q$  shortly after the coulomb explosion. At the time of detection they are in charge state  $(q + 1)$ . Left: Ions accelerated by only the extraction field ( $E_1 = 100$  V/cm) in region  $R_1$ , see lower left inset. Autoionization in between the extraction unit and magnet shifts the ions impact position as indicated for  $1 \rightarrow 1^A$  by the black arrow. Right: As left but with an additional stronger ionization field ( $E_2 = 375$  V/cm) in region  $R_2$  in order to field ionize weakly bound electrons in a given energy window, see text. Entering  $R_2$  field ionization of singly as well as higher charged ions gives rise to additional patterns ( $q^F$ ) close to the signature of the unaffected ions. Upper right inset: Calculated patterns produced by ions with nonzero recoil energy.

undergo autoionization in the field free region, a maximum of about 6% is obtained for  $q = 4$ . The  $q^F$  yields as well depend on the charge state reaching about 10% for  $q = 5$ . To roughly estimate the corresponding binding energy  $E_{\text{Ryd}}$ , principle quantum number, and orbital radius of the Rydberg electron, we consider hydrogenlike atoms but with a multiply charged core. Figure 4, right, shows the results of a corresponding quasiclassical calculation. Electrons with  $E_B < E_{\text{Ryd}}^{\text{min}}$  are field ionized already within  $R_1$ . Entering  $R_2$  electrons with  $E_B < E_{\text{Ryd}}^{\text{max}}$  are freed and the corresponding ions contribute to  $Y(q^F)$ , see Fig. 4. For example, for  $\text{Ar}^{5+}$ ,  $E_{\text{Ryd}}^{\text{min}}$  and  $E_{\text{Ryd}}^{\text{max}}$  span an energy window of roughly 50 meV. Although only a tiny binding energy range is probed by field ionization, the contribution to the signal is astonishingly high (up to 10%). Hence, HCIs with Rydberg electrons represent a considerable fraction of the emitted ions. Our findings support the theoretical result that in the Coulomb explosion a significant part of electrons appears to be weakly bound in the nanoplasma, and on a later stage of the adiabatic expansion electrons recombine to Rydberg states of the emitted ions [15]. The experimental findings demonstrate that the proposed relaxation scenario takes place even if the cluster constituents are strongly charged, e.g.,  $q$  up to 7.

In charge exchange studies on high  $q$  ions, e.g., passing a microcapillary foil, electron binding energies in the eV range have been observed [23]. Our studies verify that a CCE leads to the formation of species consisting of HCIs having electrons in meV bound states. The high abundance suggests that exploding clusters introduce a new approach to generate exotic particles like electrons in high Rydberg levels of hollow atoms [1,24]. At such low binding energy, the size of the orbit in HCIs is on the order of a hundred nanometers. Hence, CCE undergoes the evolution of a nm-sized plasma plume into a low density gas, preserving properties of a Rydberg ensemble. Phenomena like the Mott transition [25] may be addressed in future studies.

Finally, we would like to address autoionization in the field-free region of the spectrometer, see Fig. 3. As obtained in the experiment, the process takes place on a fairly long time span ranging from several tens of ns to  $\mu\text{s}$  depending on the charge state (see Fig. 5, left). Compared to characteristic time scales of a CCE (e.g., ps to reach the critical density), the corresponding average distance in between the constituents of the expanding nanoplasma is large enough to treat them as individual particles. Hence, interatomic Coulomb decay [26] as well as ionization due to dipole-dipole interaction in

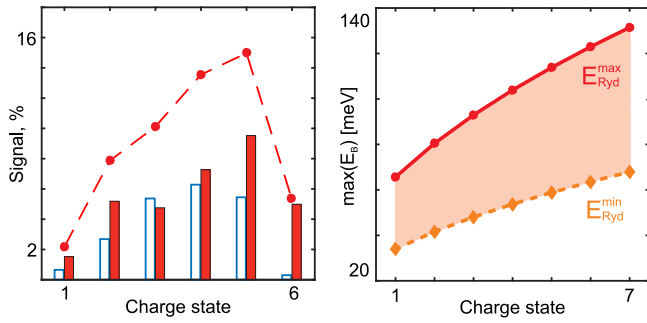


FIG. 4. Left: Abundance of ions undergoing autoionization  $Y(q^A)$  (blue open bars) and field ionization  $Y(q^F)$  (red filled bars), as extracted from Fig. 3, right. For both decay channels a considerable proportion of up to ten percent compared to the total signal is observed for each  $\text{Ar}^{q+}$ . The overall yields (dots) of these species account for a considerable fraction of the signal and peaks at about  $q = 5$  giving a value of 15%. Right: Calculated charge state dependent binding energies of electrons in high-lying Rydberg levels to be ionized by the extracting (orange diamonds line) and ionizing (red dots line) electric fields. The shaded area represents the energy window probed by the ionizing field in  $R_2$ . Lines are meant to guide the eyes.

between Rydberg ions are no potential decay channels. Since typical radiative lifetimes of electrons in excited states are on the order of ns, the observed time scale appears to be too long to allow for an Auger-like decay. Autoionizing Rydberg states (ARSs), however, as a result of the Coulomb interaction in between Rydberg and core electrons, are possible candidates to explain the experimental observations [27]. ARSs in ions have not been studied yet, in contrast with the autoionizing Rydberg series  $3p_{1/2}^5 n l'$  in neutral argon [28–32]. Calculations predict a  $n_{\text{Ryd}}^3$  dependence of the lifetime on the principal quantum number  $n$  and a  $\ell_{\text{Ryd}}^6$  dependence on the orbital quantum number  $\ell$  [33]. With respect to this scaling already at  $n_{\text{Ryd}} = 13$  and  $\ell_{\text{Ryd}} = 12$ , the expected lifetime exceeds 200 ns. In the adiabatic cooling of the nanoplasma, delocalized electrons populate localized levels of HCIs. Recombination into high- $\ell$  levels is expected as well, especially since the number of possible states is proportional to  $\ell$ . Optical excitation schemes also permits to reach high  $n_{\text{Ryd}}$ , but high- $\ell_{\text{Ryd}}$  states are hardly accessible. Assuming an increased abundance of electrons in high- $\ell_{\text{Ryd}}$  states when compared to other methods could provide an explanation for why long living ARSs in argon have not been observed yet. In order to evaluate the contribution of low- $E_B$  electrons on ARSs, the specific autoionization yields depending on  $q$  are shown in Fig. 5, right, for the two acceleration field configurations. Obviously, depopulation of electrons in high Rydberg states by field ionization in  $R_2$  shows no substantial influence on the autoionization signals. That indicates that Rydberg levels with  $E_B > E_{\text{Ryd}}^{\text{max}}$  are populated as well. In general, excess energies transferred to Rydberg electrons in ARSs are significantly higher than  $E_{\text{Ryd}}^{\text{max}}$  [34]. Hence, a considerable fraction of electrons must populate stronger bound Rydberg levels.

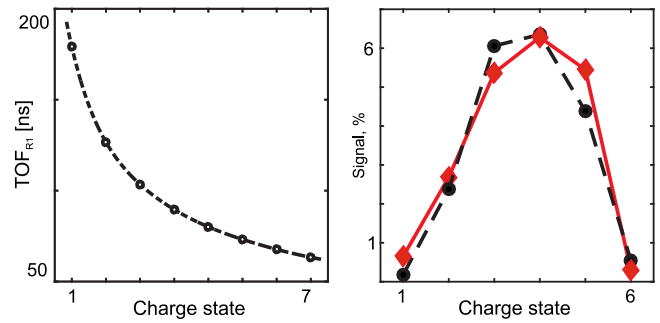


FIG. 5. Left: Maximum flight times ( $\text{TOF}_{R_1}$ ) in the first acceleration region as a function of charge state.  $\text{TOF}_{R_1}$  set lower limits for highly charged ions to undergo autoionization, see the signal of  $q^A$  in Figs. 3 and 4. The upper limit can be estimated to be in the  $\mu\text{s}$  range taking into account the TOF to the entrance of the magnet. Right: Comparison of the fraction of  $q^A$  contributing to the total yield [ $Y(q) + Y(q^F) + Y(q^A)$ ] for the extraction schemes ( $E_1$  only, circles) and ( $E_1$  and  $E_2$ , diamonds). Obviously electrons bound with energy  $E_{\text{Ryd}}^{\text{min}} < E_B < E_{\text{Ryd}}^{\text{max}}$  do not contribute to autoionization significantly.

In conclusion, the long-term behavior in the Coulomb explosion of argon clusters has been studied by means of charge and energy resolving ion spectroscopy. In the expansion of the nanoplasma, the interatomic Coulomb barriers rise and the corresponding spectra show that electrons populate high- $n_{\text{Ryd}}$  levels of ions charged up to  $q = 7$ . Hence, there is strong evidence that a Rydberg compound is formed. Significant autoionization is observed as well, caused by Coulomb interaction in between electrons in metastable Rydberg and stronger bound levels of  $\text{Ar}^{q+}$ . Its exceptional long lifetime suggests that also high- $\ell_{\text{Ryd}}$  levels are populated. However, the exact mechanism of electron localization into Rydberg states and their further dynamics remains unsolved and needs a quantum physical treatment. The described evolution of hot electrons taking place in cluster Coulomb explosions is not restricted to small particles but relevant for dense expanding plasmas in general.

The Deutsche Forschungsgemeinschaft and the Sonderforschungsbereich 652 are gratefully acknowledged for financial support. We thank S. Skruszewicz, Ch. Schaal, Th. Fennel, Ch. Peltz, and S. Scheel for fruitful discussions.

\*Corresponding author.

josef.tiggesbaeumker@uni-rostock.de.

- [1] A. McPherson, T. Luk, B. Thompson, K. Boyer, and C. Rhodes, *Appl. Phys. B* **57**, 337 (1993).
- [2] T. Ditmire, R. A. Smith, J. W. G. Tisch, and M. H. R. Hutchinson, *Phys. Rev. Lett.* **78**, 3121 (1997).
- [3] V. Kumarappan, M. Krishnamurthy, and D. Mathur, *Phys. Rev. A* **66**, 033203 (2002).
- [4] E. Springate, S. A. Aseyev, S. Zamith, and M. J. J. Vrakking, *Phys. Rev. A* **68**, 053201 (2003).

- [5] E. M. Snyder, S. A. Buzza, and A. W. Castleman, Jr., *Phys. Rev. Lett.* **77**, 3347 (1996).
- [6] M. Lezius, S. Dobosz, D. Normand, and M. Schmidt, *Phys. Rev. Lett.* **80**, 261 (1998).
- [7] T. Döppner, J. P. Müller, A. Przystawik, S. Göde, J. Tiggesbäumker, K. H. Meiwes-Broer, C. Varin, L. Ramunno, T. Brabec, and T. Fennel, *Phys. Rev. Lett.* **105**, 053401 (2010).
- [8] W. Schroeder, F. Omenetto, A. Borisov, J. Longworth, A. McPherson, C. Jordan, K. Boyer, K. Kondo, and C. Rhodes, *J. Phys. B* **31**, 5031 (1998).
- [9] R. Issac, G. Vieux, B. Ersfeld, E. Brunetti, S. Jamison, J. Gallacher, D. Clark, and D. Jaroszynski, *Phys. Plasmas* **11**, 3491 (2004).
- [10] U. Saalmann, C. Siedschlag, and J. M. Rost, *J. Phys. B* **39**, R39 (2006), and references therein.
- [11] T. Fennel, K.-H. Meiwes-Broer, J. Tiggesbäumker, P.-G. Reinhard, P. M. Dinh, and E. Surau, *Rev. Mod. Phys.* **82**, 1793 (2010), and references therein.
- [12] T. Fennel, T. Döppner, J. Passig, C. Schaal, J. Tiggesbäumker, and K.-H. Meiwes-Broer, *Phys. Rev. Lett.* **98**, 143401 (2007).
- [13] J. Passig, R. Irsig, N. X. Truong, T. Fennel, J. Tiggesbäumker, and K.-H. Meiwes-Broer, *New J. Phys.* **14**, 085020 (2012).
- [14] J. Passig, S. Zherebtsov, R. Irsig, M. Arbeiter, C. Peltz, S. Göde, S. Skruszewicz, K.-H. Meiwes-Broer, J. Tiggesbäumker, M. Kling, and T. Fennel, *Nat. Commun.* **8**, 1181 (2017).
- [15] T. Fennel, L. Ramunno, and T. Brabec, *Phys. Rev. Lett.* **99**, 233401 (2007).
- [16] T. Killian, T. Pattard, T. Pohl, and J. Rost, *Phys. Rep.* **449**, 77 (2007).
- [17] B. Schütte, M. Arbeiter, T. Fennel, M. J. J. Vrakking, and A. Rouzée, *Phys. Rev. Lett.* **112**, 073003 (2014).
- [18] B. Schütte, M. Arbeiter, T. Fennel, G. Jabbari, A. Kuleff, M. J. J. Vrakking, and A. Rouzée, *Nat. Commun.* **6** (2015).
- [19] D. Komar, K.-H. Meiwes-Broer, and J. Tiggesbäumker, *Rev. Sci. Instrum.* **87**, 103110 (2016).
- [20] D. Pentlehner, R. Riechers, B. Dick, A. Slenczka, U. Even, N. Lavie, R. Brown, and K. Luria, *Rev. Sci. Instrum.* **80**, 043302 (2009).
- [21] O. F. Hagen and W. Obert, *J. Chem. Phys.* **56**, 1793 (1972).
- [22] D. A. Dahl, *SIMION 3D Version 7.0 User's Manual* (Idaho National Engineering Laboratory, Idaho Falls, 2000).
- [23] Y. Morishita, R. Hutton, H. A. Torii, K. Komaki, T. Brage, K. Ando, K. Ishii, Y. Kanai, H. Masuda, M. Sekiguchi, F. B. Rosmej, and Y. Yamazaki, *Phys. Rev. A* **70**, 012902 (2004).
- [24] J. D. Gillaspay, *J. Phys. B* **34**, R93 (2001).
- [25] T. C. Killian, *Science* **316**, 705 (2007).
- [26] R. Santra and C. H. Greene, *Phys. Rev. Lett.* **91**, 233401 (2003).
- [27] T. F. Gallagher, *Rydberg Atoms* (Cambridge University Press, Cambridge, England, 1994).
- [28] R. E. Huffman, Y. Tanaka, and J. C. Larrabee, *J. Chem. Phys.* **39**, 902 (1963).
- [29] F. B. Dunning and R. F. Stebbings, *Phys. Rev. A* **9**, 2378 (1974).
- [30] I. D. Petrov, V. L. Sukhorukov, U. Hollenstein, L. J. Kaufmann, F. Merkt, and H. Hotop, *J. Phys. B* **44**, 025004 (2011).
- [31] J. D. Wright, T. J. Morgan, L. Li, Q. Gu, J. L. Knee, I. D. Petrov, V. L. Sukhorukov, and H. Hotop, *Phys. Rev. A* **77**, 062512 (2008).
- [32] I. D. Petrov, T. Peters, T. Halfmann, S. Aloïse, P. O'Keeffe, M. Meyer, V. L. Sukhorukov, and H. Hotop, *Eur. Phys. J. D* **40**, 181 (2006).
- [33] I. D. Petrov, V. L. Sukhorukov, and H. Hotop, *J. Phys. B* **35**, 323 (2002).
- [34] A. Kramida, Yu. Ralchenko, J. Reader, and NIST ASD Team, NIST Atomic Spectra Database (National Institute of Standards and Technology, Gaithersburg, MD.), version 5.3 (2015).